

September 3, 2005

# **Seasonal Variation of Carbon Monoxide in Northern Japan: FTIR Measurements and Source-labeled Model Calculations**

M. Koike,<sup>1</sup> N. B. Jones,<sup>2</sup> P. I. Palmer,<sup>3</sup> H. Matsui,<sup>1</sup> Y. Zhao,<sup>4</sup> Y. Kondo,<sup>5</sup> Y. Matsumi,<sup>6</sup>  
and H. Tanimoto<sup>7</sup>

<sup>1</sup> Department of Earth and Planetary Science, Graduate School of Science, The University of Tokyo, Tokyo, Japan (koike@eps.s.u-tokyo.ac.jp)

<sup>2</sup> Department of Chemistry, University of Wollongong, Wollongong, Australia

<sup>3</sup> Division of Engineering and Applied Sciences, Harvard University, Cambridge, MA, USA

<sup>4</sup> Mechanical and Aeronautical Engineering, University of California, Davis, CA, USA

<sup>5</sup> Research Center for Advanced Science and Technology, The University of Tokyo, Tokyo, Japan

<sup>6</sup> Solar-Terrestrial Environment Laboratory, Nagoya University, Aichi, Japan

<sup>7</sup> National Institute for Environmental Studies, Tsukuba, Ibaraki, Japan

Short title: KOIKE ET AL.: SEASONAL VARIATION OF CO IN JAPAN

**Submitted to Journal of Geophysical Research, Atmospheres**

**Abstract.** Tropospheric carbon monoxide (CO) was measured through out 2001 using ground-based Fourier transform IR (FTIR) spectrometer at Moshiri (44.4°N) and Rikubetsu (43.5°N) observatories in northern Japan, which are separated by 150 km. Seasonal and day-to-day variations of CO are studied using these data, and contributions from various CO sources are evaluated using three-dimensional global chemistry transport model (GEOS-CHEM) calculations. Seasonal maximum and minimum FTIR-derived tropospheric CO amounts occurred in April and September, respectively. The ratio of partial column amounts between the 0-4- and 0-12-km altitude ranges is found to be slightly greater in early spring. The GEOS-CHEM model calculations generally reproduce these observed features. Further analyses using source-labeled CO model calculations suggest that the observed seasonal variation was caused by a combination of seasonal variations of various source contributions, in addition to a seasonal change in chemical CO loss by OH. A seasonal change in the meteorological fields largely control the changes in various source contributions. The contribution from fossil fuel (FF) combustion in Asia and photochemical CO production have the greatest yearly-averaged contribution at 1 km among the CO sources (31% each). The Asian FF contribution increases from winter to summer, because weak southwesterly wind in summer brings more Asian pollutants to the observation sites. The photochemical CO production is greatest between August and December. The seasonal variation in the contribution is small ( $\pm 17\%$  at 1 km) likely due to concurrent increases (decreases) of photochemical production and loss rates in summer (winter). The contribution from inter-continental transport of European FF combustion CO is found to be comparable to that of Asian FF sources in winter. Northwesterly wind caused by the Siberian high in this season brings pollutants from Europe directly to Japan, in addition to southward transport of accumulated pollution from higher latitudes. The influences are generally greater at lower altitudes, and this vertical gradient in the contribution results in a vertical gradient

in the CO profile in winter. Model calculations underestimated CO amounts by 12-14% between March and June. Hot spots data obtained by the ATSR satellite measurements and the relationship between FTIR-derived HCN and CO amounts are generally consistent with biomass burning influences, however, quantitative estimate could not be obtained in this study.

## 1. Introduction

Quantifying the continental outflow and intercontinental transport of pollutants is one of the major challenges of atmospheric chemistry. Quantitative evaluations require accurate information regarding emissions, transport processes, and photochemical transformations. Carbon monoxide (CO) has been used to test our current knowledge because it is a good tracer of the influence from combustion processes. The lifetime of CO is sufficiently long (10 days over continents in summer to over a year at high latitudes in winter [Holloway et al., 2000]) to study how transport redistributes pollutants on a regional-to-hemispheric scale, and it is also sufficiently short that we can identify these impacts with a reasonably high signal-to-noise ratio. About half of the CO in the troposphere is estimated to be emitted directly into the atmosphere, while the other half is produced by oxidation of methane (CH<sub>4</sub>) and various volatile organic compounds (VOCs), such as isoprene [e.g., IPCC, 2001]. Of the direct CO emissions, fossil and domestic fuel burning and biomass burning are estimated to be two dominant sources. Increases in anthropogenic emissions of CO can induce an interannual trend in the CO abundance, while biomass burning is considered to be a driver of year-to-year variation of CO over hemispheric scales [Novelli et al., 2003; van der Werf et al., 2004; Yurganov et al., 2005].

Because of the rapid economic growth and industrialization in the People's Republic of China and other Asian countries, understanding the influences from anthropogenic sources in these regions is of great importance. In East Asia, impacts and transport pathways of anthropogenic emissions and biomass burning have been studied using CO [e.g., Bey et al., 2001; Liu et al., 2003; Bertsch and Jaffe, 2005; Oshima et al., 2004]. Inverse modeling techniques have also been applied to estimate CO emission amounts in East Asia and other source regions using three-dimensional chemical transport models (CTMs) and ground-based, aircraft, and satellite measurements [Palmer et al., 2003; Heald et al., 2004; and references therein]. These

studies have shown that recent emission inventories by *Streets et al.* [2003] likely underestimated anthropogenic CO emissions from China by 54%.

Quantitative understanding of anthropogenic influences on CO is especially important because of its critical role in controlling the oxidizing capacity of the atmosphere [*Logan et al.*, 1981]. The oxidation process of CO to carbon dioxide (CO<sub>2</sub>) is one of the major processes in the production of tropospheric ozone (O<sub>3</sub>). Because CO has a longer lifetime than that of most non-methane hydrocarbons (NMHCs), the relative importance of CO for photochemical ozone production is greater in the remote atmosphere. The oxidation of CO by hydroxyl (OH) radical, on the other hand, is the major sink for OH (30-60% of OH loss [*Spivakovsky et al.*, 2000]), and this reaction plays an essential role in controlling the partitioning between OH and hydroperoxy (HO<sub>2</sub>) radical.

Because of the importance of CO, surface CO concentrations have been closely watched globally since 1988 by the NOAA Climate Monitoring and Diagnostics Laboratory (CMDL) [e.g., *Novelli et al.*, 2003, 1998]. In addition to these surface measurements, a relatively long-time record of CO column abundances have been obtained by ground-based Fourier transform IR (FTIR) solar spectrum measurements, and the seasonal and year-to-year variations of CO were reported [e.g., *Rinsland et al.*, 2000, 2002; *Zhao et al.*, 2002; *Yurganov et al.*, 2005]. FTIR measurement is a unique spectroscopic technique, which can semi-continuously provide information on the vertically averaged behavior of CO, including that in the free troposphere. On the other hand, FTIR measurements can provide only little information on the vertical distribution of CO, and in general, interpretation of the CO variation has limitations due to the lack of vertical information.

Measurements of CO were made using ground-based FTIR spectrometers at two observatories in Japan (Figure 1), Moshiri Observatory (44.4°N 142.3°E, 280 m above the sea level) and Rikubetsu Observatory (43.5°N 143.8°E, 370 m above the sea

level). These two observatories are located at similar latitudes in the northern part of Japan, separated by a distance of 150 km. In this paper, we present seasonal and day-to-day variations of CO using these data. We also present contributions from various CO sources evaluated using three-dimensional global chemistry transport model (GEOS-CHEM) calculations, after showing results from a validation study of the model calculations through comparison with observations.

## 2. FTIR Measurements

Measurements of CO at Moshiri and Rikubetsu were described in detail by *Zhao et al.* [1997, 2002], and only brief descriptions are given here. High resolution solar spectra were recorded using ground-based FTIR spectrometers; a Bruker IFS 120HR with 450-cm optical path difference (OPD, or  $0.002\text{ cm}^{-1}$ , where the resolution is defined here as  $0.9/\text{OPD}$ ) and an IFS 120M with 257-cm OPD ( $0.0035\text{ cm}^{-1}$ ) at Moshiri and Rikubetsu, respectively. To improve the signal-to-noise ratio, measurements were generally made with a resolution between  $0.0028$  and  $0.0035\text{ cm}^{-1}$ . Measurements at Rikubetsu and Moshiri observatories started in 1995 and 1996 respectively, however only data obtained in the year 2001 are used in this study.

Infrared solar spectra were analyzed using the SFIT2 algorithm, which was jointly developed at the NASA Langley Research Center and the National Institute of Water and Atmosphere Research (NIWA) at Lauder, New Zealand [e.g., *Rinsland et al.*, 2000]. Using this algorithm, a vertical profile of CO is retrieved by fitting the absorption in one or more microwindows in one or more infrared solar spectra. The microwindows used to retrieve CO are given in Table 1. Note that in this study, the microwindow containing the strong CO R3 line was not used, as various tests indicated that including this window induced a non-linear response (i.e., high CO columns were underestimated) to the expected season range of CO columns. The microwindow covering the range from  $2112.08 - 2112.18\text{ cm}^{-1}$ , which contains an isolated solar CO

absorption line, was included to accurately capture solar CO absorption features that overlap all terrestrial CO lines. Spectral parameters for the retrieval analyses were taken from the 2000 HITRAN compilation [Rothman *et al.*, 2003].

For the initial vertical profile of CO used in the iterative retrieval analyses, a single profile was used for both sites for one-year data analysis based on an average of profiles obtained by in situ aircraft measurements during PEM-West A and B [Zhao *et al.*, 1997]. Daily pressure-temperature-altitude profiles at Moshiri-Rikubetsu were constructed using rawinsonde data obtained four times a day at Sapporo. For altitudes above the balloon sounding height, the 1976 US Standard Atmosphere was smoothly connected to the balloon meteorological data.

In this study, partial column amounts of CO for the 0-4- and 0-12-km altitude ranges were retrieved. We used averaged mixing ratios of CO ( $x_{\text{CO}}$ ) for these two altitude ranges, which are defined as follows.

$$x_{\text{CO}} = N_{\text{CO}} / N_{\text{air}}$$

where  $N_{\text{CO}}$  and  $N_{\text{air}}$  are the partial column amounts of CO and total air molecules, respectively. Averaging kernels for these retrievals for a typical vertical CO profile (in units of mixing ratio) is shown for solar zenith angles (SZAs) of 30° and 70° in Figure 2. The degrees of freedom (DOF) for the signal was calculated to be 1.98 for a SZA of 70° for typical atmospheric conditions, indicating that in principle, CO amounts in two altitude ranges can be independently derived.

Error analyses for these retrievals were made by examining factors listed by Zhao *et al.* [2002], and the results are given in Table 2. The greatest systematic error for the 0-4-km retrievals of 20% results from the a priori profile assumed in this study. This result indicates that the absolute values of retrieved CO amounts for the 0-12-km range are more robust than those of the 0-4-km retrievals. However, considering the DOF of 1.98, the 0-4-km retrievals provide useful information for the partitioning of the tropospheric CO column amounts between two altitude ranges, below and above 4 km.

In this study, we present averaged mixing ratios for both 0-4- and 0-12-km altitude ranges.

In the year 2001, CO data are available on 76 and 63 days for Moshiri and Rikubetsu observatories, respectively. In general, 1 to 5 spectra were recorded each day when measurements were made, and daily averages of retrieved CO amounts are used in this study. One standard deviation of the retrieved values within a day is 15% or less.

In addition to CO, we also measured and retrieved hydrogen cyanide (HCN) column amounts. HCN is known to be a good atmospheric tracer of BB [e.g., *Holzinger et al.*, 1999] and simultaneous enhancements of FTIR-derived CO and HCN column amounts likely due to influences from BB were reported [*Zhao et al.*, 2000, 2002]. Corresponding retrieval analyses are described by *Zhao et al.* [2000, 2002]. In this study we have added two extra microwindows, namely the window from 3268.18 to 3268.27  $\text{cm}^{-1}$  and 3299.46 to 3299.58  $\text{cm}^{-1}$  which contain isolated transitions of the HCN  $\nu_3$  P(14) and P(4) lines respectively. Addition of these two microwindows improves the DOFS to about 2, consistent with the CO retrieval.

### 3. Model Calculations

To evaluate the contributions of various CO sources to CO levels observed in Japan, the GEOS-CHEM global 3-D chemical transport model (CTM) is used. Detailed descriptions of the model are given elsewhere by *Palmer et al.* [2003]. Briefly, the model version used here has a horizontal resolution of  $2^\circ$  latitude  $\times$   $2.5^\circ$  longitude and has 48 vertical levels, 20 of which are below 12 km. The model is driven by assimilated meteorology from the Goddard Earth Observing System (GEOS) of the NASA Data Assimilation Office.

As CO emissions data, gridded emission inventories for anthropogenic fossil fuel and biofuel burning in East Asia provided by *Streets et al.* [2003] are used.

Because previous inversion studies suggest that anthropogenic CO emissions from China are likely to have been underestimated by 54% [Palmer *et al.*, 2003; Heald *et al.*, 2004], anthropogenic emissions from China are increased to account for this discrepancy. Fossil fuel and biofuel emissions for the rest of the world are taken from Duncan *et al.* [2003] and Yevich and Logan [2003]. For biomass burning, an inventory of the total annual biomass burned developed by J. A. Logan [Lobert *et al.*, 1999] is used with a climatological seasonal apportionment that was developed by Duncan *et al.* [2003] using Along Track Scanning Radiometer (ATSR, 1996-2000) and Advanced Very High Resolution Radiometer (AVHRR, 1992-1994) satellite observations. The interannual variability for 2001 activity in the northern Asia and eastern Russia (45°-70°N and 80°-180°E) was computed using ATSR satellite data and was found to be close to an averaged activity. In addition to direct emissions of CO, there is a large photochemical production of CO in the atmosphere from the oxidation of methane (CH<sub>4</sub>) and non-methane volatile organic compounds (NMVOCs). Because anthropogenic and biomass burning NMVOCs are in general co-emitted with CO, the primary emissions of CO were correspondingly increased by 20% (fossil fuel) and 10% (biofuel and biomass burning). For oxidation of methane and biogenic NMVOCs, the model includes sources of methane (850 Tg CO/yr), isoprene (175 Tg CO/yr), methanol (85 Tg CO/yr), and some other VOCs. For the CO sink, only the reaction CO + OH is considered, and monthly mean OH concentration fields calculated from a full-chemistry simulation are used.

To study contributions of various CO sources to the CO levels observed in Japan, we conducted a “source-labeled” (or “source-tagged”) CO simulation. In this simulation, a CO amount is expressed by a linear sum of contributions from fossil fuel burning (FF) and biomass burning (BB) in individual geographical regions. This source-label information is tracked and contributions from various CO sources can be evaluated at any location and time. Because a total CO amount does not change when

source-label information is added, this treatment will not affect levels of other species and therefore, we can use the fixed OH levels described above. For FF CO, emissions in Asia, Europe, North America, and other regions (Figure 1a) are resolved. For BB CO, emissions in Asia, Africa, South America, and other regions are resolved. In addition, photochemically produced CO is labeled.

Results from model calculations were saved every hour, and we use daytime averages (0600 to 1800 solar local time) for the present analyses. Because of the limited vertical resolution of the FTIR CO measurements, model-calculated values were averaged vertically using the averaging kernels, shown in Figure 2, as follows.

$$\tilde{x} = (A - I)x_0 + Ax$$

where,  $x_0$  is a vector of the initial vertical profile of CO used for the FTIR retrieval analyses,  $x$  is a vector of model-calculated values,  $\tilde{x}$  is a vector of averaged values to be compared with observations,  $A$  is the averaging kernel matrix, and  $I$  is a unit matrix. Because the vertical shape of an averaging kernel changes with SZA (Figure 2), the SZA at which measurements had been made was averaged for individual days and an averaging kernel for this averaged SZA was used for each day.

## 4. Results

### 4.1. Comparison of the Two FTIR Measurements

Measurements of CO were made at both Moshiri and Rikubetsu on the same day on 25 total days in 2001. In Figure 3a, a scatter plot between the CO values observed at these two sites (0-4-km retrieval) is shown. In general, these two measurements agreed to within a root-mean-square (RMS) difference of 12 parts per billion by volume (ppbv) or 7.2%, with an  $r^2$  value of 0.75. A linear fit to the data results in a slope of 1.04 with a small intercept (-2.1 ppbv). The agreement between the two measurements indicates that the overall errors in the measurements are within the estimated uncertainties, confirming the validity of the measurements. The agreement also indicates that CO observations at these sites are not affected by local CO sources, and results can be considered to represent CO values in the northern Japan over an area with a horizontal scale of over 150 km, the distance between the two observatories. Considering the spatial resolution of the GEOS-CHEM model of  $2^\circ \times 2.5^\circ$ , this result indicates that it is reasonable to make a direct comparison between the measurements and model calculations. In the following analyses, we combined the Moshiri and Rikubetsu data and refer to them as Moshiri-Rikubetsu data hereafter; if only one of the two data sets is available, it is used, and if both data sets are available, an average is taken. As a result, the subset of available data increases to a total of 114 days.

FTIR-derived CO values at Moshiri are also compared with in situ surface measurements made at Rishiri Island Observatory ( $45.1^\circ\text{N}$ ,  $141.1^\circ\text{E}$ ), which is located 130 km north of the Moshiri observatory (Figure 3b). In situ CO measurements were made using a modified non-dispersive infrared (NDIR) photometer instrument (Kimoto, model 541) [Tanimoto *et al.*, 2002a]. For cases in which in situ CO concentrations are lower than 200 ppbv, no apparent systematic bias is found between the measurements. This result further confirms the validity of FTIR measurements and retrieval for the

0-4-km altitude range. This result also suggests that the CO partial column for the 0-4-km retrieval generally shows similar behavior to that of surface CO. When CO concentrations are greater than 200 ppbv, CO values at the surface are systematically higher than the FTIR 0-4-km retrieval values, which is likely due to greater enhancement of CO near the surface.

## 4.2. Seasonal Variation

In Figure 4, a time series of daily 0-4-km CO mean mixing ratio values from Moshiri-Rikubetsu retrieval is shown. Monthly averages of 0-4 and 0-12 km are also shown in Figure 5 and given in Table 3. As also listed in Table 3, 8 to 16 daily data are available for individual months. As seen in these figures and table, a seasonal maximum and minimum appear in spring (April) and early fall (September), respectively. The monthly averages in April and September for the 0-4-km retrievals are 192 and 136, ppbv, respectively. The seasonal variation of tropospheric CO, with its maximum in winter/early spring and minimum in summer, is observed over the globe [e.g., *Novelli et al.*, 1992, 1998; *Rinsland et al.*, 2000, 2002; *Zhao et al.*, 2002]. It is largely driven by the seasonal variation in OH concentration; smaller OH concentrations and hence a longer lifetime of CO during winter result in an accumulation of CO toward spring until loss by OH surpasses inputs of CO (emissions and photochemical production). Seasonal variations of emission strength and transport also cause seasonal variations in the CO concentrations depending on the location of the measurements. Surface CO measurements made by NOAA/CMDL indicate that the maximum and minimum northern hemispheric averaged CO concentrations appear in March and July, respectively [*Novelli et al.*, 1998]. Compared with these results, the seasonal minimum appears in slightly later (September) at Moshiri-Rikubetsu. A seasonal minimum around September was also observed by ground surface measurements at Rishiri Island [*Tanimoto et al.*, 2002b]. As discussed later in section

5.1, changes in both photochemistry and transport pattern cause the observed seasonal minimum in the northern Japan.

In Figure 6, a ratio of partial column amounts between the 0-4 km and 0-12 km altitude ranges is shown. A seasonal maximum and minimum appear in February-March and August, respectively, indicating that a seasonal increase in CO in the lower troposphere is slightly greater compared to that in the middle-upper troposphere in late-winter/early-spring, while the contrast in CO mixing ratio between the lower and upper altitudes becomes smaller in late summer. Because the DOF is nearly 2 ( $SZA = 70^\circ$ ) for the FTIR retrievals in this study, it is possible to derive the seasonal tendency in the vertical structure of the CO profile, although the vertical resolution of the FTIR measurements and retrieval analyses is limited. During summer a vertical gradient in the CO profile is expected to diminish through vertical mixing, while during winter a vertical change in anthropogenic influences results in vertical gradients in the CO profile, as will be discussed later in more detail in section 4.5.

### **4.3. Comparison with GEOS-CHEM Model**

Model-calculated CO amounts (daily and monthly) are compared with Moshiri-Rikubetsu observations in Figures 4 and 5. As described in section 2, model-calculated values were smoothed using averaging kernels from the FTIR retrieval analyses so that direct comparison with observations can be made. To calculate monthly averages, only model results on days when observation data are available (that are shown in Figure 4) are used. As seen in these figures, the GEOS-CHEM model generally reproduced the observed seasonal variations well. The RMS differences between the daily values and the monthly averages for the 0-4-km retrievals are 22 ppbv (14%) and 17 ppbv (11%), respectively, which is within the combined uncertainties in the absolute value of the observations and model calculations. An  $r^2$  value for the monthly averages is 0.80 (0-4 km) and 0.78 (0-12 km). An underestimation by the

model is found between March and June for both the 0-4- and 0-12-km altitude ranges. For the 0-4-km range, the model underestimates the observations by 21-27 ppbv or 12-14% during this time period. One of the possible explanations for this difference is an underestimation of the BB contribution in the model, as discussed later in section 5.3.

In Figure 6, the model-calculated partial column ratio between the 0-4-km and 0-12 km altitude ranges is compared with observations. In general, a good agreement in absolute value and its seasonal variation is found, suggesting that the model calculation successfully reproduced the processes driving the seasonal variation in the vertical structure of the CO profile.

It is noted that the GEOS-CHEM model successfully reproduced observed day-to-day variation in various cases. For example, the model captured pronounced increases on days 100, 145, 169, and 218-219, with lower values around each event. Considering the lifetime of CO ranges from a few weeks to several months, the agreement in the day-to-day variation indicates that the transport process and the emission inventory in the model are generally good.

The agreement with CO observations in absolute value, seasonal variations, day-to-day variations, and in the ratio of partial column amounts between the 0-4- and 0-12-km altitude ranges confirm the validity of the model calculations. In the following sections, results from the “source-labeled” CO simulations are presented, and processes which contribute to these observed variations are discussed.

#### **4.4. Individual Source Contributions**

In this section, results from “source-labeled” CO simulations for Moshiri and Rikubetsu observatories are presented, and contributions from various CO sources are described. In Figure 7, a time series of model-calculated daily CO values is shown at a sigma level of 0.90 (altitude of about 1 km) where sigma level is defined as follows.

$$\sigma = \frac{p - p_T}{p_s - p_T}$$

where  $p$  is atmospheric pressure level at which CO concentrations are calculated in the model,  $p_s$  is atmospheric pressure at the surface, and  $p_T$  is atmospheric pressure at the top boundary of the model (0.001 hPa in this calculation). In Figure 7, various source contributions (results from “source-labeled” simulations) are also shown. For this plot, results for all days in the year 2001 are shown, irrespective of the date of observation. In Figure 8, monthly averages are shown. When yearly averaged contributions at 1 km are examined (Table 4), the contributions from Asian FF combustion and photochemical production are the greatest (31% each). Contributions from European FF combustion (18%) and that from North American FF combustion (9%) follow. A very small but non-zero contribution from South American BB is considered to be resulted from episodic transport events across the equator.

As seen in Figures 7 and 8, seasonal variation in the modeled CO is caused by a complex interaction between various CO source contributions. The contribution from Asian FF combustion increases from January to July (38 to 72 ppbv) and is greatest between May and July. Its contribution suddenly decreases between July and August by a factor of about 2 (72 to 34 ppbv), and it stays relatively constant for the rest of the year. These seasonal changes can generally be interpreted as changes in the origin of transported air parcels caused by seasonal variation in the meteorological fields over East Asia, as discussed later in section 5.1. It is evident that most of the day-to-day variations in total CO values are due to Asian FF combustion. This is presumably because CO emission sources are close to the observatories and air parcels influenced by these emission sources are transported to the observatories without significant dilution. Consequently, day-to-day variation of transport processes directly cause day-to-day variations of CO concentrations.

Contributions from European and North American FF combustion are large

between October and April, with a maximum contribution appearing around January at an altitude of 1 km. It is noted that in winter months, the European contribution is comparable to that from Asian FF combustion, indicating that inter-continental long-range transport maintains the observed high CO levels. The large contributions from long-range transport in the winter months is likely due to the longer CO lifetime and favorable wind patterns, as discussed later in section 5.2.

The contribution from biomass burning in Asia is generally large between April and September. As noted above, a climatological source distribution and strength were used for this calculation. The yearly averaged contribution is 6%. The contributions from biomass burning in Africa and South America were found to be less than 2%.

The contribution from photochemical CO production from oxidation of methane and NMVOCs has a comparable yearly averaged contribution (31%) to that of Asian FF combustion at an altitude of 1 km, as described above. Oxidation of methane by OH is the dominant pathway of photochemical production of CO, and short-lived biogenic NMVOCs make only small contributions. Between August and December, the contribution from photochemical CO production is greatest within the CO sources considered in this study. In August and September especially, this contribution is dominant (44 and 49%, respectively, of the total CO). When the absolute amount of the photochemical contribution is examined, the greatest contribution appears in July-August, in accordance with the highest photochemical activities, while the minimum contribution appears in April. It is noted that the contribution is 40-60 ppbv throughout the year (or  $\pm 17\%$  change from the average), and it does not necessarily decrease significantly during winter, in spite of a more-than-a-factor-of-20 reduction in OH concentration near the surface at mid-latitudes (e.g., 0.9 and  $23.1 \times 10^5$  molecules  $\text{cm}^{-3}$  in January and July, respectively, at 900 hPa and 44°N [Spivakovsky *et al.*, 2000]). This is likely because both photochemical production and loss are smaller in winter than in summer. Although the chemical production rate of CO is low in winter,

thus-produced CO molecules are considered to be accumulating throughout the winter, due to the long CO lifetime.

#### **4.5. Vertical Profiles of Individual Source Contributions**

Vertical profiles of various source contributions at Moshiri-Rikubetsu are shown in Figures 9a and 9b for January and July, respectively. As seen in these figures, contributions from various sources have different vertical structure and seasonal variations. Here we examine these features for individual sources.

The contribution from Asian FF combustion decreased remarkably in summer from 1 to 2 km by a factor of about 2 (76 to 41 ppbv) and another factor of 2 (41 to 23 ppbv) from 2 to 4 km. This vertical change essentially makes a vertical gradient of CO concentration (sum of individual contributions) in this altitude range. This kind of large change in the lower troposphere cannot be seen in January (38 and 28 ppbv at 1 and 4 km, respectively). Large vertical changes in spring and summer months were likely due to influences from horizontal transport of CO within the boundary layer from sources in Japan and neighboring countries (see discussion about transport pathway for summer months in section 5.1.). In the free troposphere, a less pronounced vertical gradient is found both in July and January for the Asian FF combustion contribution.

A contribution from European FF combustion decreases with altitude throughout the troposphere in January (46 and 18 ppbv at 1 and 6 km, respectively). The absolute value of the reduction in this altitude range is greater than those of the other CO sources (Asian FF contribution is 38 and 27 ppbv at 1 and 6 km, respectively). As a consequence, the vertical gradient of the CO profile in January is primarily due to the vertical gradient of the European FF contribution (Figure 9a). As described above in section 4.2, a seasonal maximum of the partial column ratio of CO between 0-4 and 0-12 km appears in February-March in both observations and model calculations (Figure 6), suggesting that the vertical gradient of CO concentration is greatest in

late-winter/early-spring. The results presented in this study suggest that the most important driver of this seasonal change in the vertical CO column fraction is the inter-continental transport of European FF CO. During summer, the contribution is much smaller, especially within the boundary layer, and the maximum contribution appears in the free troposphere (around 5 km, Figure 9b). The very small contribution in the boundary layer in summer is because meteorological conditions are not favorable for direct transport of European air parcels to Japan (section 5.2.) and because the photochemical lifetime of CO is short near the surface

Photochemical production of CO shows only a small decrease with altitude both in summer and winter (20-30% reduction from the surface to the tropopause). The lack of vertical dependence was likely because both production and loss rates are larger at lower altitudes. A small seasonal variation in the photochemical contribution is likely because both production and loss rates are large in summer, as described in the previous section.

## **5. Discussion**

### **5.1. Transport Pathways and Influence from Asian Fossil Fuel Combustion**

In Figures 10a and 10b, the mean wind field at 925 hPa ( $\approx 1$  km) is shown for January and July. In Figures 11a and 11b, 10-day kinematic back trajectories starting from over Moshiri at an altitude of 1 km are shown. Color coding shows the atmospheric pressure of air parcels along the trajectories. For this calculation, meteorological data provided by the European Centre for Medium-Range Weather Forecasts (ECMWF) on a  $2.5^\circ \times 2.5^\circ$  latitude-longitude grid were used. As seen in these figures, in January, northerly winds dominated over the northern Japan due to the Siberian high. As a result, air over far-east Siberia was generally transported to the Moshiri-Rikubetsu region, and some direct transport from the north of Europe within 10 days are also seen. In July, southwesterly winds are seen over the Moshiri-Rikubetsu

region, and the wind speed is generally lower than that in January. As a result, air masses arriving at low altitudes generally had stagnated around Japan and the Japan Sea, so that they received emissions over Japan and the eastern rim of the Asian continent. Note that there is a relatively large uncertainty in the individual trajectory calculations for air parcels arriving at 1 km due to vertical mixing of air within the planetary boundary layer. However, the general features of the trajectories in each season are considered to be captured by these calculations.

To study the locations of emission sources that could have affected air parcels arriving at the Moshiri-Rikubetsu region in more detail, CO emissions that individual air parcels received along trajectories were integrated at each emission grid box (Figures 11a and 11b). In this calculation, the total time duration in which individual air parcels existed in each grid box at altitudes below the 800-hPa level was calculated and it was multiplied by the CO emissions for this particular grid. Emission inventory provided by *Streets et al.* [2003] increased by a factor of 1.54 (see description in section 3) was used for East Asia. The EDGAR 1995 emission inventory [*Olivier et al.*, 2001; <http://arch.rivm.nl/env/int/coredata/edgar/>] was used for the rest of the world because of its high spatial resolution ( $1^\circ \times 1^\circ$  in latitude and longitude). Because the absolute amount of calculated values does not have physical meaning, arbitrary units are chosen for these figures to show relative source contributions from various regions. As seen in these figures, in January, emissions from the east rim region of the Asian continent facing the Rikubetsu-Moshiri region contributed to the increase of the CO level in addition to emissions within the northern Japan. In contrast, in July, emission sources over a wide region in Japan, the Korean Peninsula, and the northeastern part of China contributed to the CO abundance in the northern Japan. This seasonal change in the locations of the dominant source regions was due to a shift of wind direction from northerly to southwesterly, as described above (Figures 10a and 10b). This wind regime shift caused a greater contribution of Asian fossil fuel combustion CO sources in

July as compared with that in January at 1 km, as already described in section 4.4 (Figure 8). When the seasonal variation of wind regime from winter to summer is examined month by month, the mean wind direction is found to change from northerly (winter) to westerly (spring) and to southwesterly (summer), causing a gradual increase in Asian fossil fuel contributions.

As described in the previous section (section 4.5), a sharp decrease in CO concentration with increasing altitude in the lower troposphere in July is likely due to a sharp decrease in Asian FF contributions (Figure 9). Although the vertical mixing of air is efficient during summer, the direct horizontal transport of pollutants within the boundary layer from sources in Japan and neighboring countries still induce this feature.

In August, the mean wind at 925 hPa weakened and shifted to the southeasterly direction, which brought cleaner maritime air to the Moshiri-Rikubetsu region (not shown), resulting in a factor-of-2 reduction in Asian FF contributions from July to August (Figure 8), as described in section 4.4. Between September and December, the wind direction at 925 hPa changed to westerly and then to northwesterly while increasing in speed. A slightly higher Asian FF contribution in October and November than in previous and subsequent months (Figure 8) resulted from transport of anthropogenic CO by the westerlies that appeared in these two months.

As described in section 4.2, a seasonal minimum of CO in the northern Japan appears slightly later than the northern hemispheric average (September versus July) derived from NOAA/CMDL surface CO measurements [Novelli *et al.*, 1998]. As shown above, July is the month when the influence from Asian FF combustion is quite large, because of southwesterly winds. In August and September, cleaner air is transported to the northern Japan, resulting in a seasonal minimum. Meteorological conditions, in addition to photochemistry, likely cause the difference in seasonal variation.

## 5.2. Influence from European Fossil Fuel Combustion

European FF contributions are comparable to those of Asian FF contributions in winter months at Moshiri-Rikubetsu at 1 km (Figure 8). The contributions decrease with increasing altitude with a factor-of-2.5 reduction between 1 and 6 km in January (Figure 9a). This vertical gradient of European FF contributions resulted in a vertical gradient in the CO profile in winter, and this process was likely responsible for the observed seasonal maximum of the partial column ratio of CO between 0-4 and 0-12 km in February-March (Figure 6 and description in section 4.5). The large contribution in the winter lower troposphere is considered to be due to the following two factors. First, because of the long chemical lifetime of CO at high latitudes during winter, CO emitted into the atmosphere accumulated, resulting in the inter-continental impact. Emitted CO could have circulated the globe at northern high latitudes by the circumpolar westerlies before arriving at the Moshiri-Rikubetsu region. Weak vertical transport processes during the winter caused higher European FF contributions at lower altitudes. Second, clockwise circulation around the Siberian high caused direct transport of air parcels influenced by European CO sources to the Moshiri-Rikubetsu region. This airflow can be seen in trajectories of air parcels arriving at Moshiri-Rikubetsu (Figure 11a). The descending motion of air through the circulation around the Siberian high resulted in higher contributions from European fossil fuel combustion at lower altitudes, resulting in the vertical gradient in the contributions shown in Figure 9a. The direct transport process can be identified in the relatively large day-to-day variation of European fossil fuel contributions shown in Figure 7. In other words, the transport process is an episodic event, which can take place when the meteorological fields are favorable. This is in contrast to the North American FF contributions, which do not show a clear day-to-day variation, indicating that direct transport is small and the contributions are likely due to accumulation at high latitudes as described above.

The fossil fuel contributions both from Europe and North America are smaller between May and September as compared with those in the rest of the year at 1 km altitude (Figure 8). The smaller contributions are again consistent with the shift in the wind regime near the surface (southerly wind during later summer and early fall) and shorter photochemical lifetime of CO. When the vertical profile of contributions from European fossil fuel combustion is examined for July conditions (Figure 9b), the maximum is found in the free troposphere (around 5 km), although its absolute values are much smaller than those in January (Figure 9a). Although southwesterly wind is seen near the surface, westerly winds dominate in the free troposphere which brings air parcels influenced by European sources (not shown).

### **5.3. Possible Influences from Boreal Forest Fire**

The model calculations underestimate CO amounts between March and June by 21-27 ppbv (12-14%) (Figure 5). One of the possible explanations for this discrepancy is an underestimation of BB contributions such as those from far-east Russia. The year-to-year variability for the year 2001 activity in northern Asia and eastern Russia (45°-70°N and 80°-180°E) was computed using ATSR satellite data and was found to be close to an average activity. However, due to uncertainty in our estimation and the year-to-year variation of BB regions, it is worthwhile to examine this hypothesis.

In Figure 13, hot spots detected by ATSR satellite measurements [*Stricker et al.*, 1995] are shown for April 2001 with back trajectory of the air parcels arriving at Moshiri at 1 km altitude. As seen in this figure, there were some BB activities in far-east Russia in the region centered around 50°N and 125°E, and air parcels that could have been influenced by these activities were transported to the Moshiri-Rikubetsu region by northwesterly winds. Although the number of hot spots in this region is greater in July-August as for intensive forest fire events in 1998 [*Kajii et al.*, 2002;

*Zhao et al.*, 2002], the impact to Moshiri-Rikubetsu CO can be greater in earlier months, due to the wind patterns in the lower troposphere. Some BB activities can also be found in the north-western part of China centered around 65°N and 75°E (Figure 13), and air parcels that had passed over this region also reached the Moshiri-Rikubetsu region. Therefore, hot spot data and air parcel trajectories suggest that air parcels arriving at Moshiri-Rikubetsu were likely to be affected by BB sources in spring.

In this study, we also examined the relationship between the CO and HCN amounts derived by FTIR measurements, because HCN is known to be a good atmospheric tracer of BB [e.g., *Holzinger et al.*, 1999]. HCN is produced by BB and residential coal burning and is likely to be lost by ocean uptake and reaction with OH, with a tropospheric lifetime of 5 months [e.g., *Li et al.*, 2000, 2003; *Singh et al.*, 2003]. As seen in Figure 14, there is a positive correlation between daily CO and HCN column amounts. In this figure, data are shown only for selected months so that changes due to seasonal variations of CO and HCN are minimized within individual time periods. *Zhao et al.* [2002] reported that simultaneous enhancements of FTIR-derived CO and HCN column amounts were observed at Moshiri-Rikubetsu between August and October 1998 and that they were likely due to influences from BB over far-east Russia. In the present study, a ratio of enhancements (anomalies from the normal seasonal variation) between HCN and CO ( $\Delta\text{HCN}/\Delta\text{CO}$ ) are calculated for data obtained in the year 1998 and 2002 using the method described by *Zhao et al.* [2002]. As for the year 1998 [*Zhao et al.*, 2002; *Novelli et al.*, 2003; *van der Werf et al.*, 2004; *Yurganov et al.*, 2004], large enhancements in CO likely due to boreal forest fires in Russia were observed in the year 2002 [*Yurganov et al.*, 2005]. As a result, a slope of 1.27-1.28 pptv / ppbv was obtained for both 1998 and 2002 data (a heavy solid line in Figure 14), that is slightly smaller than the value reported by *Zhao et al.* [2002] of 1.60 pptv/ppbv. As seen in Figure 14, ratios of increases between HCN and CO observed in April and May 2001 are generally similar to the ratio obtained in 1998 and 2002, and therefore

they are consistent with BB influences.

When HCN data are used as a BB source indicator however, other sources should be also considered. *Singh et al.* [2003] and *Li et al.* [2003] reported that there is a systematic difference in ratios of the increase in HCN with that in CO between BB plumes and Chinese urban plumes (the latter are likely due to residential coal burning), based on in situ measurements during TRACE-P. The slopes reported by these authors are also shown in Figure 14. As seen in this figure, the slope for 1998 and 2002 anomalies, which were likely due to BB, is closer to the “urban plume” slope rather than “biomass burning” slope observed during TRACE-P. This result suggests that a  $\Delta\text{HCN}/\Delta\text{CO}$  slope close to that for 1998 and 2002 anomalies is not necessarily an evidence of BB influences. Furthermore, laboratory and field fire studies reveal that the emission ratio of HCN relative to CO in BB varies by 2 orders of magnitude, depending on fire type, burnt biomaterials, and the phase of the fire [*Yokelson et al.*, 1996, 1997; *Holzinger et al.*, 1999]. Considering also uncertainties in the observations, present results indicate that it is hard to identify influences from BB solely using the observed  $\Delta\text{HCN}/\Delta\text{CO}$  ratios and quantify its influence on the CO budget.

In summary, the results from both hot spot analyses and analyses using HCN data are not inconsistent with BB influences in spring. Considering a relatively small contribution from Asian BB of 7-11% (including BB in far-east Russia, see Figure 1) for the time period when the model underestimates the observations (March-June), BB activities in far-east Russia or other regions could have contributed more to the observed CO levels than those in the model calculations. However to quantify the BB source strength more accurately, further investigations by performing multi-year model calculations should be done.

## 6. Conclusions

Tropospheric CO measurements were made throughout 2001 using ground-based FTIR spectrometers at Moshiri (44.4°N 142.3°E) and Rikubetsu observatories (43.5°N 143.8°E) in northern Japan, which are separated by 150 km. CO amounts at altitude ranges of 0-4 and 0-12 km were retrieved using the vertical profile retrieval algorithm SFIT2. Retrieved CO amounts in the 0-4-km layer obtained at the two observatories agreed within uncertainties, indicating that observed CO values were not affected by local sources and can be considered to represent CO levels in northern Japan. Reasonable agreement was also found between the 0-4-km retrieved values and in situ CO measurements, except for pollution transport events (surface CO > 200 ppbv), providing further support corroborating the FTIR measurements.

Seasonal maximum and minimum FTIR-derived tropospheric CO amounts occurred in April and September, respectively (192 and 136 ppbv for the 0-4-km retrieval). The ratio of partial column amounts between the 0-4- and 0-12-km altitude ranges was found to be slightly greater in early spring. The GEOS-CHEM model calculations generally reproduced these observed features, although model calculations underestimated observations between March and June.

Contributions from various CO sources, such as anthropogenic FF combustion, BB, and photochemical production from CH<sub>4</sub> and NMVOCs were evaluated using source-labeled CO model calculations. The results presented in this study show that the observed seasonal variation was caused by a combination of seasonal variations of various source contributions in addition to a seasonal change in CO loss by reaction with OH. The contribution from Asian FF combustion increased from January to July, and it decreased by a factor of about 2 between July and August, staying relatively constant for the rest of the year. Trajectory analysis of observed air parcels indicated that a seasonal change in the meteorological fields largely controlled the changes in these contributions. Weak southwesterly winds during summer brought more Asian

pollution to Moshiri-Rikubetsu than in other seasons. Most of the day-to-day variations in CO values were also found to be due to those of the Asian FF contributions.

The inter-continental transport of European FF combustion CO was found to be comparable to Asian FF sources in winter at 1 km altitude. In this season, northwesterly wind caused by the Siberian high brought pollutants from Europe directly to Japan, in addition to southward transport of accumulated pollution from higher latitudes. The influences were generally greater at lower altitudes because of the descending motion of air. This vertical gradient of European FF contributions resulted in a vertical gradient in the CO profile in winter, and this process was likely responsible for the observed seasonal maximum of the partial column ratio of CO between 0-4 and 0-12 km in February-March.

The contribution from photochemical CO production from oxidation of CH<sub>4</sub> and NMVOCs was greatest between August and December, among the CO sources considered in this study. When the absolute amount of the photochemical contribution was examined, the greatest contribution appeared in July-August, in accordance with the highest photochemical activities. The seasonal change in the contribution was only  $\pm 17\%$  likely because both photochemical production and loss are greater in summer than in winter. The photochemical contribution also had small vertical variations both in summer and winter (20-30% reduction from surface to tropopause), likely because both production and loss rates are larger in lower altitudes.

When the yearly averaged contributions at 1 km were examined, the contribution from Asian FF combustion and photochemical production were the greatest (31% each). The contribution from European FF combustion (18%) and that from North American FF combustion (9%) followed.

Model calculations underestimated CO amounts by 12-14% between March and June. Hot spots data obtained by the ATSR satellite measurements and the

relationship between FTIR-derived HCN and CO amounts are generally consistent with BB influences in spring, however, quantitative estimate could not be obtained in this study. Because the year-to-year variation of tropospheric CO is largely controlled by BB CO emissions, further study is needed to evaluate their impacts on the budget of CO.

**Acknowledgements.**

The authors would like to thank M. Sera, Y. Ikegami, and H. Hanano for their assistance in the FTIR observations at Moshiri and Rikubetsu. The kind and helpful cooperation of the town of Rikubetsu is also greatly appreciated. The authors wish to acknowledge the public use of the ATSR World Fire Atlas. The meteorological data were supplied by the European Centre for Medium-Range Weather Forecasts (ECMWF). This work was supported in part by the Ministry of Education, Culture, Sports, Science, and Technology (MEXT). The trajectory calculation program used in this paper was developed by Y. Tomikawa and K. Sato at the National Institute of Polar Research, Japan.

## References

- Bey, I., D. J. Jacob, J. A. Logan, and R. M. Yantosca (2001), Asian chemical outflow to the Pacific in spring: Origins, pathways, and budgets, *J. Geophys. Res.*, *106*, 23,097-23,113.
- Bertschi, I. T., and D. A. Jaffe (2005), Long-range transport of ozone, carbon monoxide, and aerosols to the NE Pacific troposphere during the summer of 2003: Observations of smoke plumes from Asian boreal fires, *J. Geophys. Res.*, *110*, D05303, doi:10.1029/2004JD005135.
- Duncan, B. N., R. V. Martin, A. C. Staudt, R. Yevich, and J. A. Logan (2003), Interannual and seasonal variability of biomass burning emissions constrained by satellite observations, *J. Geophys. Res.*, *108*(D2), 4100, doi:10.1029/2002JD002378.
- Heald, C. L., et al. (2004), Comparative inverse analysis of satellite (MOPITT) and aircraft (TRACE-P) observations to estimate Asian sources of carbon monoxide, *J. Geophys. Res.*, *109*, D23306, doi:10.1029/2004JD005185.
- Holloway, T., H. L. Levy II, and P. Kasibhatla (2000), Global distribution of carbon monoxide, *J. Geophys. Res.*, *105*, 12,123-12,147.
- Holzinger, R., C. Warneke, A. Hansel, A. Jordan, and W. Lindinger (1999), Biomass burning as a source of formaldehyde, acetaldehyde, methanol, acetone, acetonitrile, and hydrogen cyanide, *Geophys. Res. Lett.*, *26*, 1161-1164.
- Intergovernmental Panel on Climate Change (IPCC) (2001), *Climate change 2001: The scientific basis*, Geneva.
- Kajji et al. (2002), Boreal forest fires in Siberia in 1998: Estimation of area burned and emissions of pollutants by advanced very high resolution radiometer satellite data, *J. Geophys. Res.*, *107*(D24), 4745, doi:10.1029/2001JD001078.
- Li, Q., D. J. Jacob, I. Bey, R. M. Yantosca, Y. Zhao, Y. Kondo, and J. Northolt (2000), Atmospheric hydrogen cyanide (HCN): Biomass burning source, ocean sink ?, *Geophys. Res. Lett.*, *27*, 357-360.
- Li, Q., D. J. Jacob, R. M. Yantosca, C. L. Heald, H. B. Singh, M. Koike, Y. Zhao, G. Sachse, and D. Streets (2003), A global three-dimensional model analysis of the atmospheric budgets of HCN and CH<sub>3</sub>CN: Constraints from aircraft and ground measurements, *J. Geophys. Res.*, *108*(D21), 8827, doi:10.1029/2002JD003075.

- Liu, H., D. J. Jacob, I. Bey, R. M. Yantosca, B. N. Duncan, and G. W. Sachse (2003), Transport pathways for Asian combustion outflow over the Pacific: Interannual and seasonal variations, *J. Geophys. Res.*, *108*(D20), 8786, doi:10.1029/2002JD003102.
- Lobert, J., W. Keen, J. Logan, and R. Yevich (1999), Global chlorine emissions from biomass burning: Reactive chlorine emissions inventory, *J. Geophys. Res.*, *104*, 8373-8389.
- Logan J. A., M. J. Prather, S. C. Wofsy, and M. B. McElroy (1981), Tropospheric chemistry: A global perspective, *J. Geophys. Res.*, *86*, 7210-7254.
- Novelli, P. C., P. Steele, and P. P. Tans (1992), Mixing ratios of carbon monoxide in the troposphere, *J. Geophys. Res.*, *97*, 20,731-20,750.
- Novelli, P. C., K. A. Masarie, and P. M. Lang (1998), Distributions and recent changes of carbon monoxide in the lower troposphere, *J. Geophys. Res.*, *103*, 19,015-19,033.
- Novelli, P. C., K. A. Masarie, P. M. Lang, B. D. Hall, R. C. Myers, and J. W. Elkins (2003), Reanalysis of tropospheric CO trends: Effects of the 1997-1998 wildfires, *J. Geophys. Res.*, *108*(D15), 4464, doi10.1029/2002JD003031.
- Olivier, J.G.J. and J.J.M. Berdowski (2001) Global emissions sources and sinks. In: Berdowski, J., Guicherit, R. and B.J. Heij (eds.) "The Climate System", pp. 33-78. A.A. Balkema Publishers/Swets & Zeitlinger Publishers, Lisse, The Netherlands. ISBN 90 5809 255 0.
- Oshima, N., M. Koike, H. Nakamura, Y. Kondo, N. Takegawa, Y. Miyazaki, D. R. Blake, T. Shirai, K. Kita, S. Kawakami, and T. Ogawa (2004), Asian chemical outflow to the Pacific in late spring observed during the PEACE-B aircraft mission, *J. Geophys. Res.*, *109*, D23S05, doi:10.1029/2004JD004976.
- Palmer, P. I., D. J. Jacob, D. B. A. Jones, C. L. Heald, R. M. Yantosca, J. A. Logan, G. W. Sachse, and D. G. Streets (2003), Inverting for emissions of carbon monoxide from Asia using aircraft observations over the western Pacific, *J. Geophys. Res.*, *108*(D21), 8828, doi:10.1029/2003JD003397.
- Rinsland, C. P., E. Mahieu, R. Zander, P. Demoulin, J. Forrer, and B. Buchmann (2000), Free tropospheric CO, C<sub>2</sub>H<sub>6</sub>, and HCN above central Europe: Recent

- measurements from the Jungfraujoch station including the detection of elevated columns during 1998, *J. Geophys. Res.*, *105*, 24,235-24,249.
- Rinsland et al (2002), Multiyear infrared solar spectroscopic measurements of HCN, CO, C<sub>2</sub>H<sub>6</sub>, and C<sub>2</sub>H<sub>2</sub> tropospheric columns above Lauder, New Zealand (45°S latitude), *J. Geophys. Res.*, *107*, doi10.1029/2001JD001150.
- Rothman, L. S. et al. (2003), The HITRAN molecular spectroscopic database: Edition of 2000 including updates through 2001, *J. Quant. Spectrosc. Radiat. Transfer*, *82*, 5-44.
- Singh, H. B., et al. (2003), In situ measurements of HCN and CH<sub>3</sub>CN over the Pacific Ocean: Source, sink, and budgets, *108(D20)*, 8795, doi:10.1029/2002JD003006.
- Spivakovsky et al. (2000), Three-dimensional climatological distribution of tropospheric OH: Update and evaluation, *J. Geophys. Res.*, *105*, 8931-8980.
- Streets, D. G., et al. (2003), An inventory of gaseous and primary aerosol emissions in Asia in the year 2000, *J. Geophys. Res.*, *108(D21)*, 8809, doi:10.1029/2002JD003093.
- Tanimoto, H., H. Furutani, S. Kato, J. Matsumoto, Y. Makide, and H. Akimoto (2002a), Seasonal cycles of ozone and oxidized nitrogen species in northeast Asia, 1. Impact of regional climatology and photochemistry observed during RISOTTO 1999-2000, *J. Geophys. Res.*, *107(D24)*, 4747, doi:10.1029/2001JD001496.
- Tanimoto, H., O. Wild, S. Kato, H. Furutani, Y. Makide, Y. Komazaki, S. Hashimoto, S. Tanaka, and H. Akimoto (2002b), Seasonal cycles of ozone and oxidized nitrogen species in northeast Asia, 2. A model analysis of the roles of chemistry and transport, *J. Geophys. Res.*, *107(D23)*, 4706, doi:10.1029/2001JD001497.
- van der Werf, G. R., J. T. Randerson, G. J. Collatz, L. Giglio, P. S. Kashibhatla, A. F. Arellano Jr., S. C. Olsen, and E. S. Kasischke (2004), Continental-scale partitioning of fire emissions during the 1997 to 2001 El Nino/La Nina period, *Science*, *303*, 73-76.
- Yevich, R., and J. A. Logan (2003), An assessment of biofuel use and burning of agricultural waste in the developing world, *Global Biogeochemical Cycles*, *17(4)*, doi:10.1029/2002GB001952.
- Yokelson, R. J., D. W. T. Griffith, and D. E. Ward (1996), Open-path Fourier transform infrared studies of large scale laboratory biomass fires, *J. Geophys. Res.*, *101*,

21,067-21,080.

- Yokelson, R. J., R. Susott, D. E. Ward, J. Reardon, and D. W. T. Griffith (1997), Emissions from smoldering combustion of biomass measured by open-path Fourier transform infrared spectroscopy, *J. Geophys. Res.*, 102, 18,865-18,877.
- Yurganov et al. (2004), A quantitative assessment of the 1998 carbon monoxide emission anomaly in the Northern Hemisphere based on total column and surface concentration measurements, *J. Geophys. Res.*, 109, D15305, doi:10.1029/2004JD004559.
- Yurganov et al. (2005), Increased Northern Hemispheric carbon monoxide burden in the troposphere in 2002 and 2003 detected from the ground and from space, *Atmos. Chem. Phys.*, 5, 563-573.
- Zhao, Y., Y. Kondo, F.J. Murcray, X. Liu, M. Koike, K. Kita, H. Nakajima, I. Murata, and K. Suzuki (1997), Carbon monoxide column abundances and tropospheric concentrations retrieved from high resolution ground-based infrared solar spectra at 43.5 ° N over Japan, *J. Geophys. Res.*, 102, 23,403-23,411.
- Zhao, Y., Y. Kondo, F.J. Murcray, X. Liu, M. Koike, H. Irie, K. Suzuki, M. Sera, and Y. Ikegami, Seasonal variations of HCN over northern Japan measured by ground-based infrared solar spectroscopy, *Geophys. Res. Lett.*, 27, 2085-2088, 2000.
- Zhao, Y., K. Strong, Y. Kondo, M. Koike, Y. Matsumi, H. Irie, C. P. Rinsland, N. B. Jones, K. Suzuki, H. Nakajima, H. Nakane, and I. Murata (2002), Spectroscopic measurements of tropospheric CO, C<sub>2</sub>H<sub>6</sub>, C<sub>2</sub>H<sub>2</sub>, and HCN, in northern Japan, *J. Geophys. Res.*, 107(D18), 4343, doi:10.1029/2001JD000748.

## Authors' addresses

- N. B. Jones, Department of Chemistry, University of Wollongong, Wollongong, NSW 2522, Australia (njones@uow.edu.au).
- M. Koike and H. Matsui, Department of Earth and Planetary Science, Graduate School of Science, The University of Tokyo, Hongo 7-3-1, Bunkyo-ku, Tokyo, 113-0033, Japan (koike@eps.s.u-tokyo.ac.jp, matsui@eps.s.u-tokyo.ac.jp).
- Y. Kondo, Research Center for Advanced Science and Technology, University of Tokyo, 4-6-1 Komaba, Meguro, Tokyo 153-8904, Japan (kondo@atmos.rcast.u-tokyo.ac.jp).
- Y. Matsumi, Solar-Terrestrial Environment Laboratory, Nagoya University, Toyokawa, Aichi, Japan (matsumi@stelab.nagoya-u.ac.jp).
- P. I. Palmer, Division of Engineering and Applied Sciences, Harvard University, Pierce Hall, 29 Oxford Street, Cambridge MA 02138, USA (pip@io.harvard.edu).
- H. Tanimoto, National Institute for Environmental Studies, 16-2 Onogawa, Tsukuba, Ibaraki 305-8506, Japan (tanimoto@nies.go.jp).
- Y. Zhao, Mechanical and Aeronautical Engineering, University of California, Davis, CA, USA (yzhao@evolene.engr.ucdavis.edu).

## Figure Captions

Figure 1. (a) Source regions for “source-labeled” CO tracer simulations. (b) Geographic locations of Moshiri and Rikubetsu observatories.

Figure 2. Averaging kernels for 0-4- and 0-12-km CO retrievals for solar zenith angles (SZAs) of 30° and 70°.

Figure 3. (a) Scatter plot of observed daily CO mixing ratio ratios (0-4-km retrievals) between Moshiri and Rikubetsu measurements. (b) Scatter plot of observed daily CO mixing ratios between Moshiri (0-4-km retrievals) and Rishiri (in situ measurements at the surface).

Figure 4. Daily CO mixing ratios in the year 2001 obtained by FTIR observation (0-4-km retrievals; combined data for Moshiri and Rikubetsu) and corresponding GEOS-CHEM model calculations on days when observed data are available. Model results were vertically smoothed using averaging kernels so that their values can be directly compared.

Figure 5. Monthly averages of CO mixing ratios in the year 2001 obtained by FTIR observation (0-4- and 0-12-km retrievals; combined data for Moshiri and Rikubetsu) and corresponding GEOS-CHEM model calculations. For the model calculations, only the results for days when observed data are available are used after vertical smoothing using averaging kernels.

Figure 6. Ratio of partial column amounts between 0-4- and 0-12-km altitude ranges. For the model calculations, only the results for days when observed data are available are used after the vertical smoothing using averaging kernels.

Figure 7. Model-calculated daily CO values at a sigma level of 0.902 (about 1 km altitude) at Moshiri-Rikubetsu, in northern Japan. Contributions from various CO sources are also shown. Results for all days in the year 2001 are shown. No smoothing is applied. Notation (source-label) is explained in Table 4.

Figure 8. Model-calculated monthly CO values at a sigma level of 0.902 (about 1 km altitude) at Moshiri-Rikubetsu, in northern Japan. Contributions from various CO sources are also shown. Notation (source-label) is explained in Table 4. Results for all days in the year 2001 are used.

Figure 9. Vertical profile of model-calculated monthly averaged CO values at Moshiri-Rikubetsu, in northern Japan in January and July. Contributions from various CO sources are also shown. Notation (source-label) is explained in Table 4. Results for all days in the year 2001 are used.

Figure 10. Monthly mean horizontal wind field at 925 hPa ( $\approx 1$  km) in January and July (ECMWF  $2.5^\circ \times 2.5^\circ$  grid data).

Figure 11. Back trajectories of air parcels arriving at Moshiri at 1 km altitude in January and July. Trajectories for individual days are shown. Color coding shows the atmospheric pressure of air parcels along the trajectories.

Figure 12. Map showing integrated CO emissions that individual air parcel received within individual grid boxes along trajectories in January and July. The total time duration in which individual air parcels existed in each grid box at altitudes below the 800-hPa level was calculated and it was multiplied by the CO emissions for this particular grid box.

Figure 13. Hot spots detected by ATSR satellite measurement in April 2001 and back trajectory of air parcels arriving at Moshiri at 1 km altitude. Trajectories are shown for only one for every three days.

Figure 14. Scatter plot between observed daily CO mixing ratios (0-12-km retrievals) and daily HCN mixing ratios (0-12-km retrievals) at Moshiri-Rikubetsu (combined data) for selected months. A slope of enhancements (anomalies from the normal seasonal variation) between HCN and CO ( $\Delta\text{HCN}/\Delta\text{CO}$ ) calculated for data

obtained in the year 1998 and 2002 using the method described by *Zhao et al.* [2002] is also shown (heavy solid line). Slopes derived from in situ observations during TRACE-P in biomass burning plumes, and Chinese urban plumes (the latter are likely due to residential coal burning) are also shown [*Singh et al.*, 2003; *Li et al.*, 2003].

Table 1. Microwindows used for CO and HCN retrievals

Line identification	Line Center cm <sup>-1</sup>	Spectral Region cm <sup>-1</sup>	Interfering Absorption
†CO(1-0) P(10)	2057.8575	2057.684-2058.0	O <sub>3</sub> , CO <sub>2</sub> , OCS
†CO(1-0) P(7)	2069.6559	2069.56-2069.76	O <sub>3</sub> , CO <sub>2</sub> , OCS
*CO(6-5) R(32)	2112.1452	2112.08-2112.18	O <sub>3</sub>
HCN (3-0) P(14)	3268.2229	3268.18-3268.27	H <sub>2</sub> <sup>17</sup> O, H <sub>2</sub> <sup>18</sup> O
HCN (3-0) P(8)	3287.2483	3268.18-3268.27	
HCN (3-0) P(4)	3299.5273	3299.46-3299.58	H <sub>2</sub> O, O <sub>3</sub>

† The absorption is due to the isotope <sup>13</sup>C<sup>16</sup>O.

\* The absorption is due to solar CO.

Table 2. Error budget for CO and HCN retrievals (%)

	CO		HCN
	0-4 km	0-12 km	0-12 km
Systematic Error			
Forward model approximation	4	4	2
Spectroscopic parameters	2	2	5
Instrumental line shape	1.2	1.2	1
A priori profile	20	6	15
Total (RSS)	21	7.6	16
Random Error			
Spectral noise	4	2	6
SZA	<1	<1	<1
Temperature	4.2	4.2	3.2
Interference	<1	<1	<1
Total (RSS)	6.0	4.9	6.9

Table 3. Monthly average CO mixing ratios in the year 2001 obtained by FTIR observations (combined data for Moshiri and Rikubetsu)

Month	N	CO 0~4 km (ppbv)		CO 0~12 km (ppbv)	
		Average	$\sigma$	Average	$\sigma$
1	7	165	8	131	7
2	9	175	9	137	6
3	8	189	12	149	11
4	8	192	12	152	9
5	16	189	18	152	15
6	9	173	18	141	15
7	8	145	10	120	7
8	12	155	15	128	12
9	13	136	16	111	12
10	14	150	21	118	14
11	10	141	8	112	6
12	0	-----	-----	-----	-----

Table 4. Results from source-labeled model calculation of CO at sigma levels of 0.902 and 0.464 (about 1 and 6 km altitude) at Moshiri-Rikubetsu.

Source	Contribution (%)					
	$\sigma = 0.902$			$\sigma = 0.464$		
	Yearly Average	January	July	Yearly Average	January	July
<b>Fossil Fuel</b>						
Asia (AS_FF)	30.9	22.8	44.9	19.3	22.1	19.8
Europe (EU_FF)	17.7	27.5	3.9	13.1	15.6	9.8
North America (NA_FF)	8.8	13.0	2.5	11.6	14.4	6.6
Other (Other_FF)	1.7	3.1	0.6	2.7	3.8	1.3
<b>Biomass Burning</b>						
Asia (AS_BB)	5.8	2.0	5.9	5.7	2.4	8.5
Africa (AF_BB)	1.4	1.7	0.7	3.0	3.2	1.5
South America (SA_BB)	0.6	0.7	0.4	1.3	1.1	0.9
Other (Other_BB)	2.5	1.6	1.7	2.4	1.6	3.6
Chemical Production	30.6	27.6	39.4	41.0	35.8	48.0

Figure1

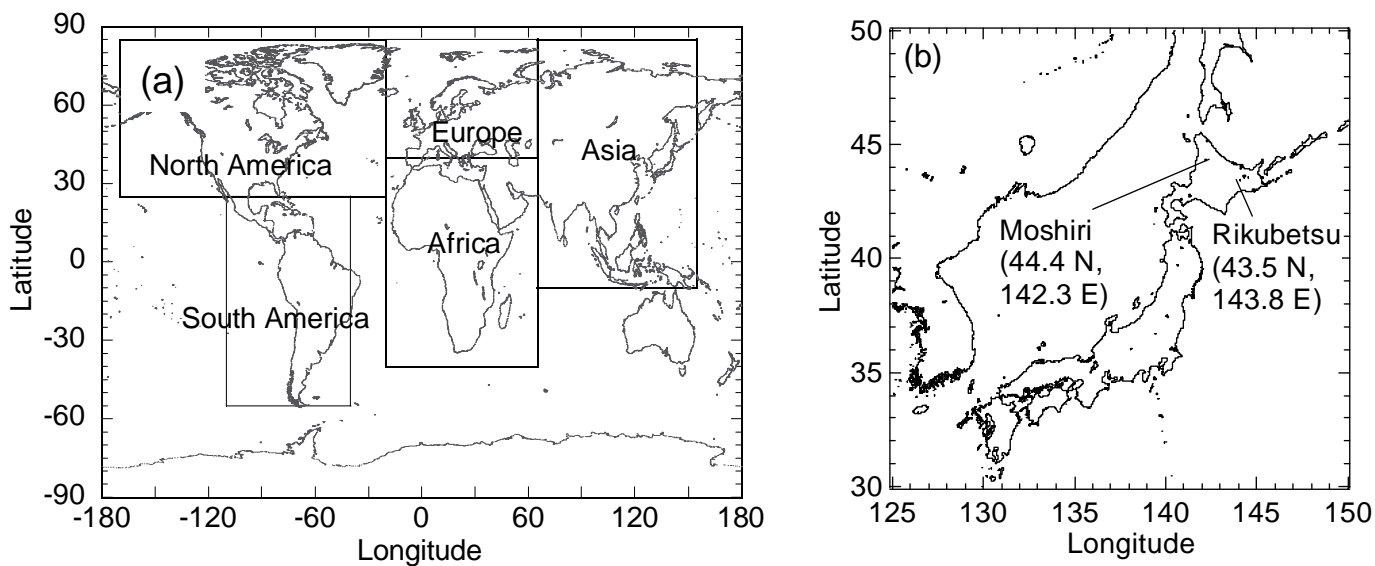


Figure2

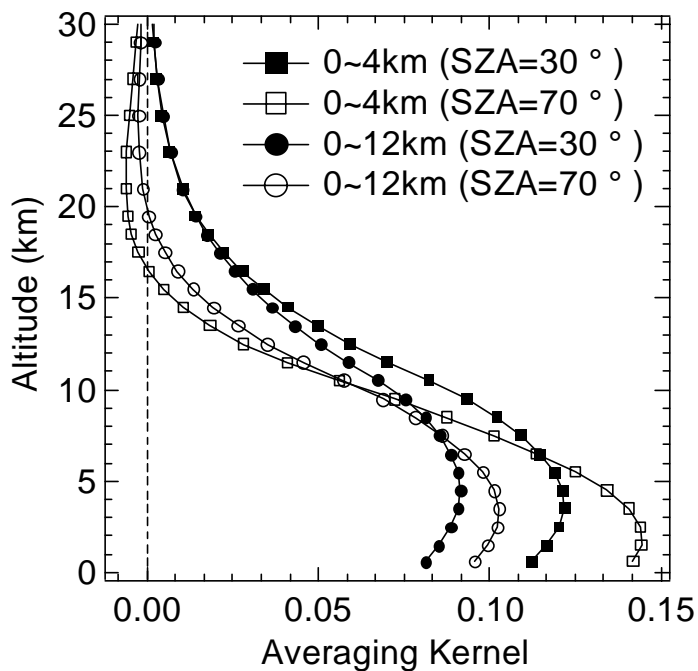


Figure3

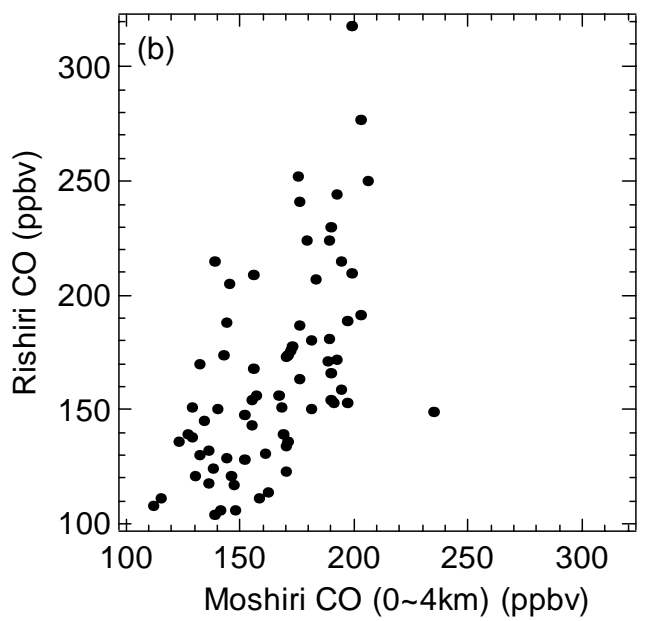
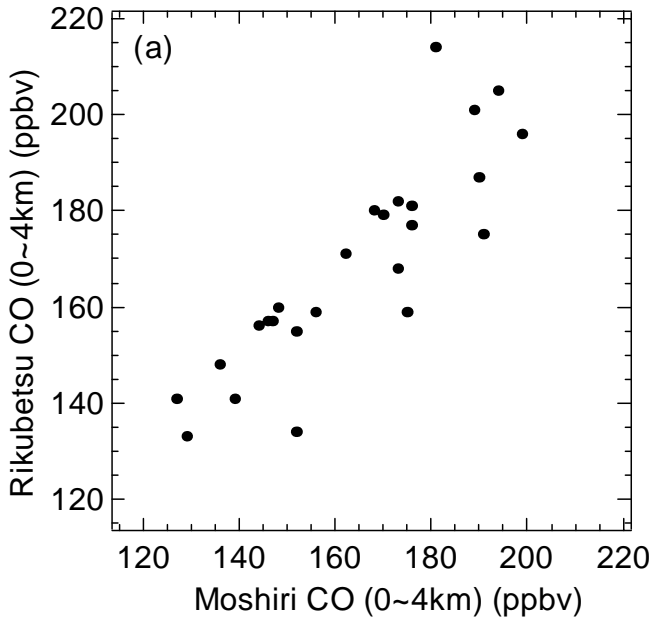


Figure4

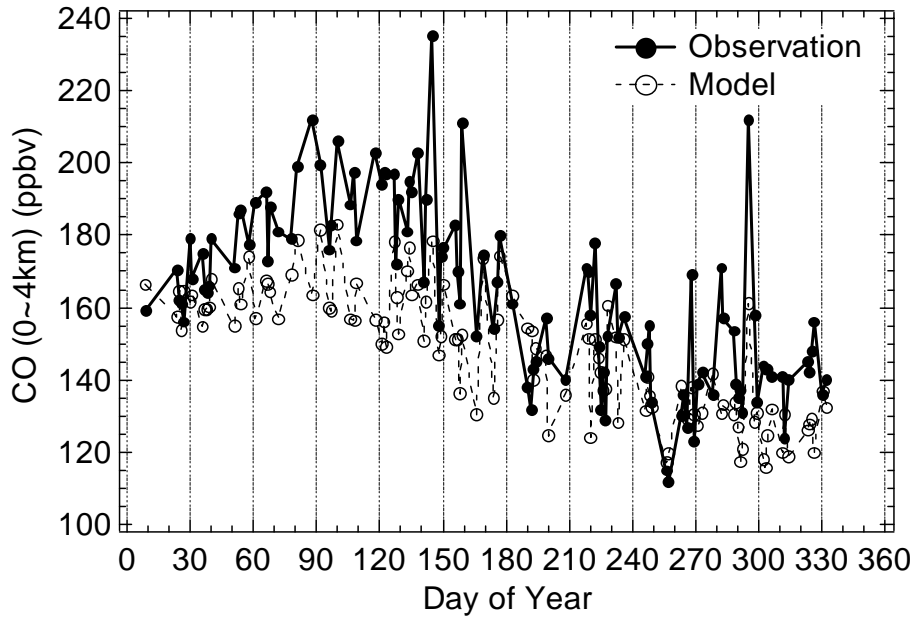


Figure5

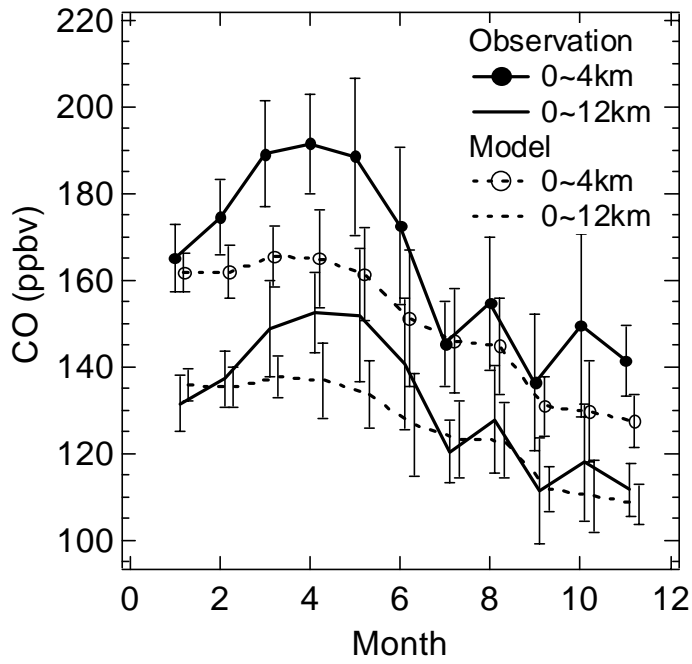


Figure6

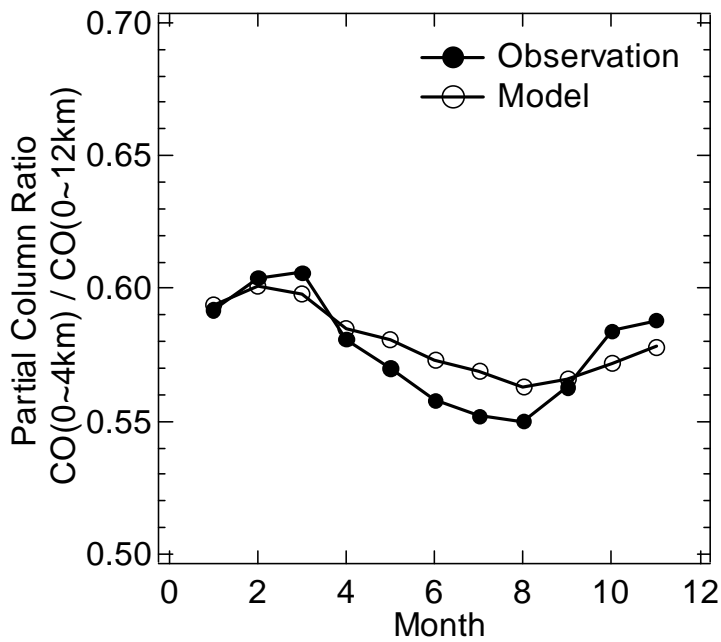


Figure7

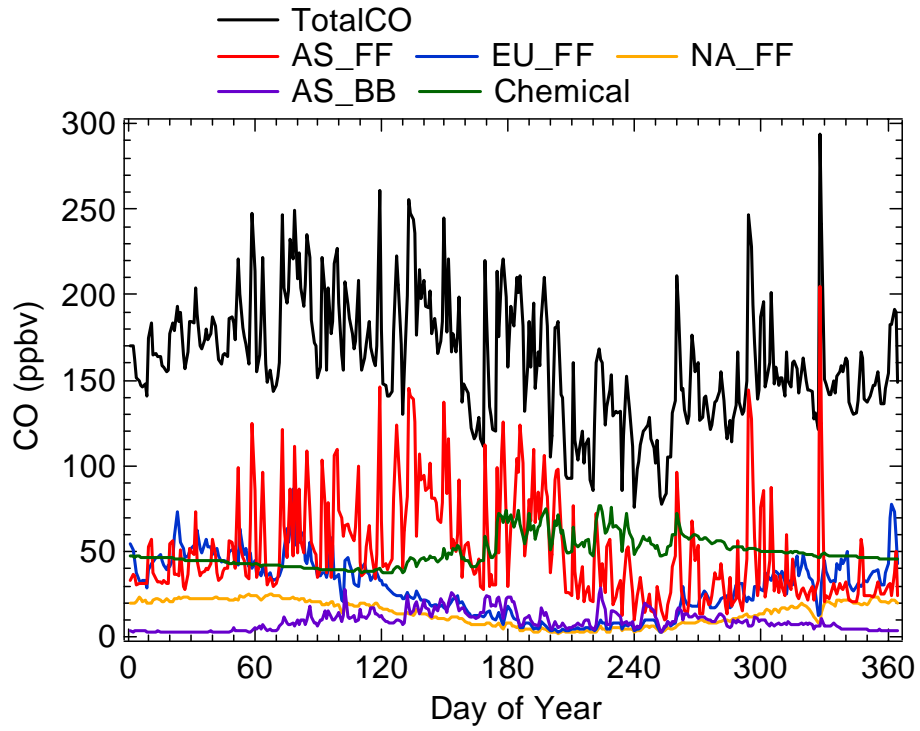


Figure8

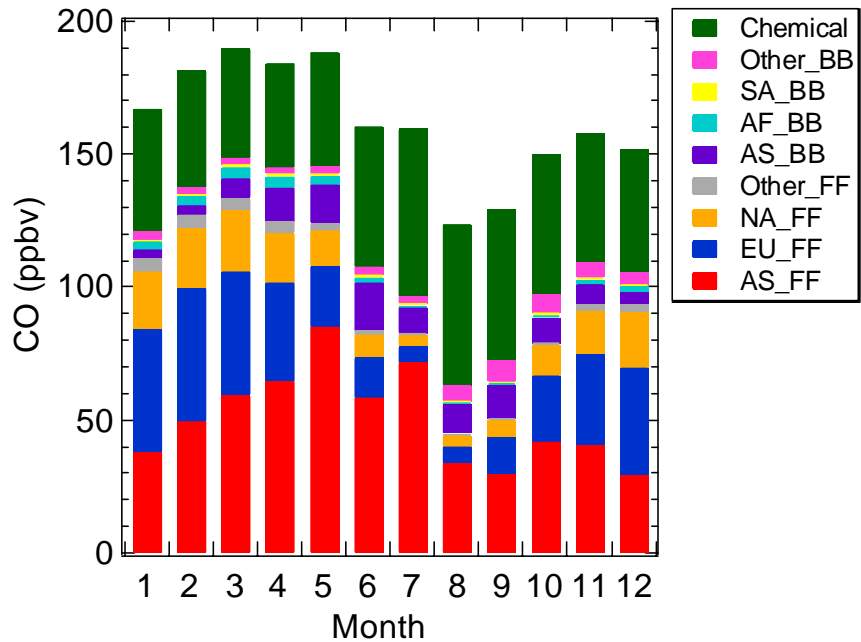


Figure9

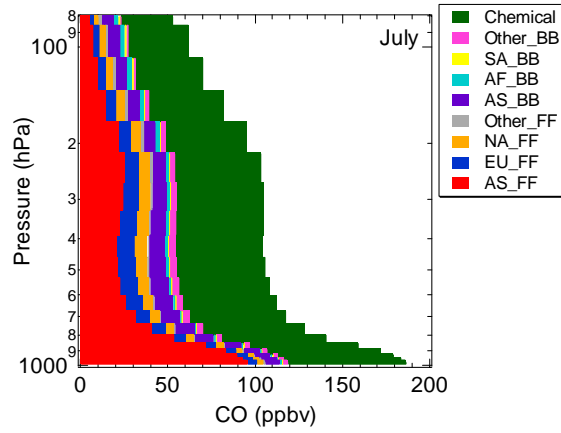
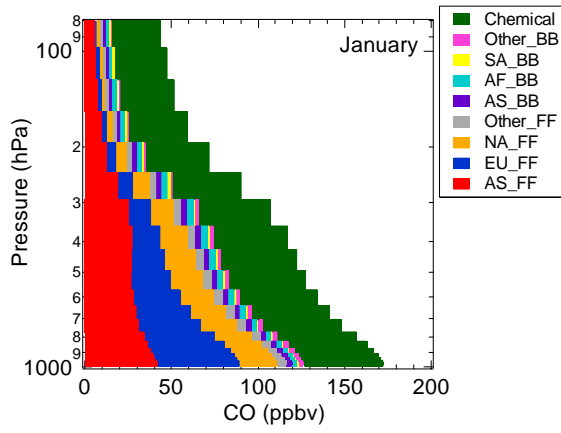
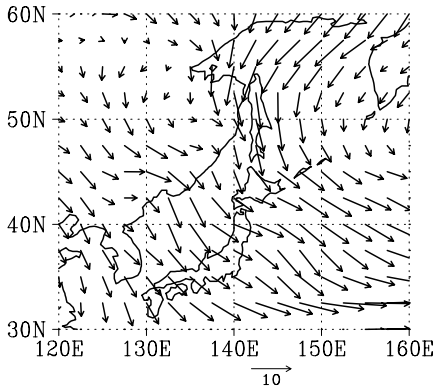


Figure10

(a) JAN 2001 Mean Wind at 925 hPa



(b) JUL 2001 Mean Wind at 925 hPa

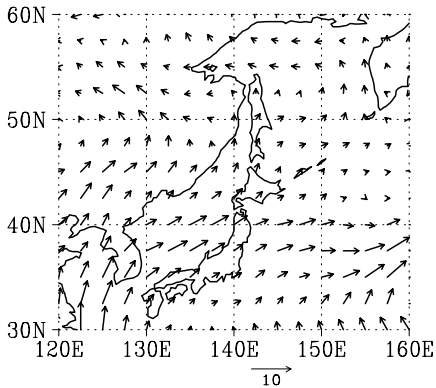


Figure11

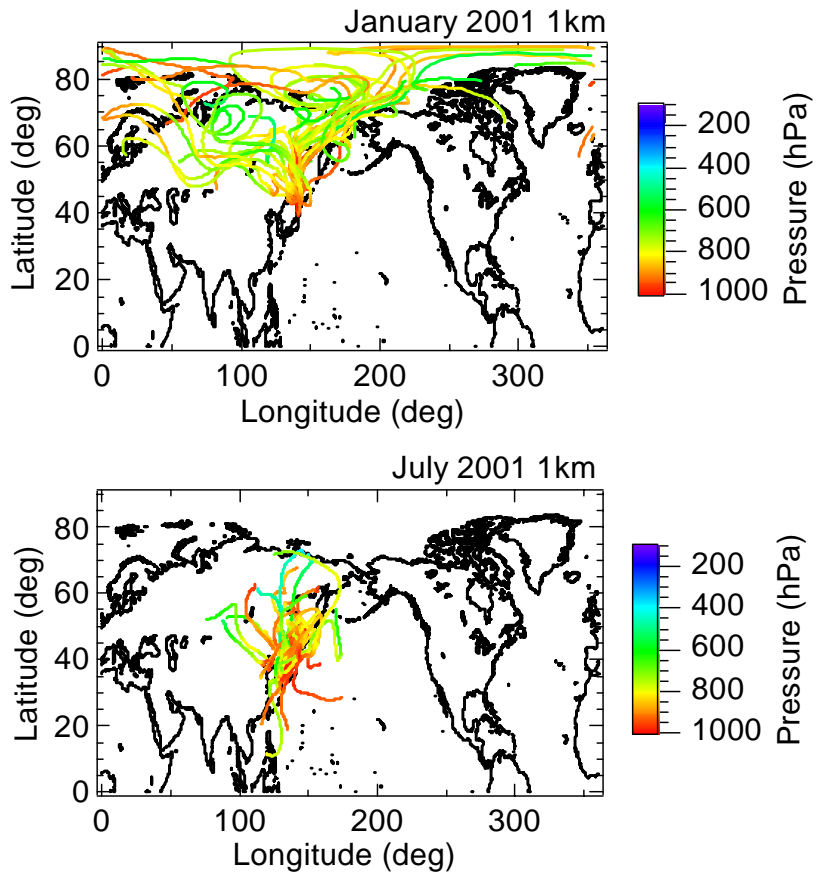


Figure12

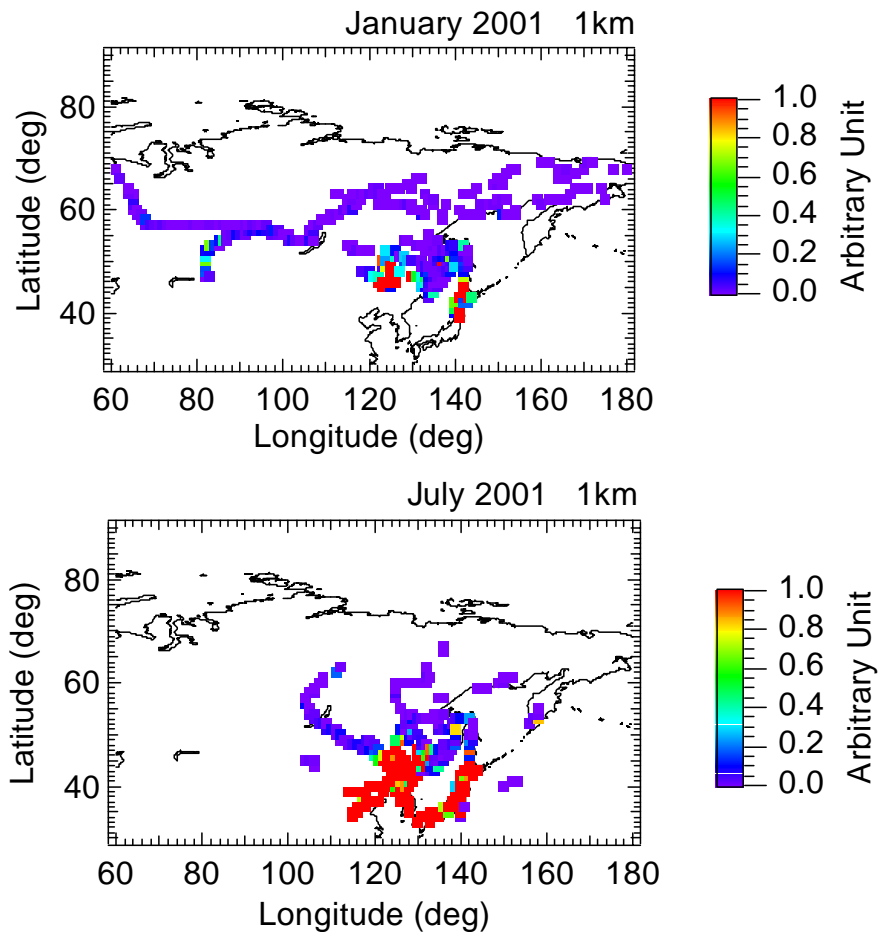


Figure13

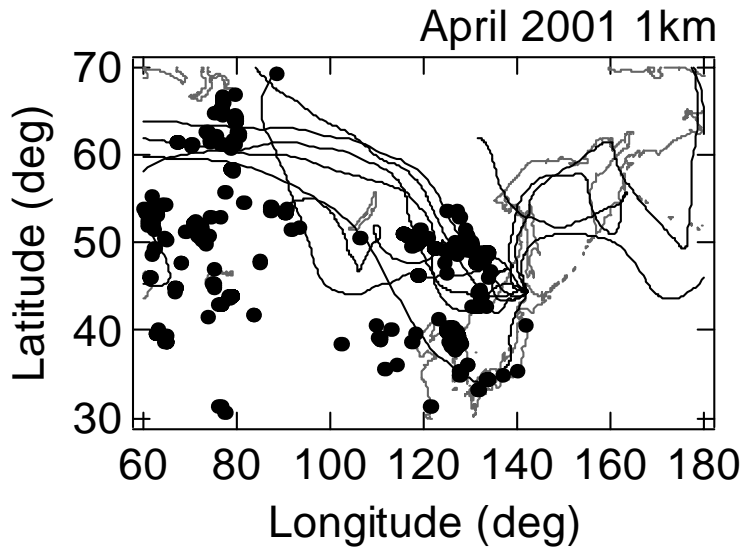


Figure14

